Research Article | Vol. 25, No. 2 | 23 Jan 2017 | OPTICS EXPRESS 720

Optics EXPRESS

# Relative change measurement of physical quantities using dual-wavelength coherent OTDR

SASCHA LIEHR,[1,*] YONAS SEIFU MUANENDA,[2] SVEN MÜNZENBERGER,[1] AND KATERINA KREBBER[1]

[1]*Bundesanstalt für Materialforschung und –prüfung (BAM), Unter den Eichen 87, 12205 Berlin, Germany*
[2]*Scuola Superiore Sant'Anna, TeCIP Institute, 56124 Pisa, Italy*
**sascha.liehr@bam.de*

**Abstract:** We propose the use of alternating pulse wavelengths in a direct-detection coherent optical time domain reflectometry (C-OTDR) setup not only to measure strain and temperature changes but also to determine the correct algebraic sign of the change. The sign information is essential for the intended use in distributed mode shape analysis of civil engineering structures. Correlating relative backscatter signal shifts in the temporal/signal domain allows for measuring with correct magnitude and sign. This novel approach is simulated, experimentally implemented and demonstrated for temperature change measurement at a spatial resolution of 1 m.



**OCIS codes:** (060.2370) Fiber optics sensors; (280.1350) Backscattering; (290.5870) Scattering, Rayleigh.

## References and links

1. S. V. Shatalin, V. N. Treschikov, and A. J. Rogers, "Interferometric optical time-domain reflectometry for distributed optical-fiber sensing," Appl. Opt. **37**(24), 5600–5604 (1998).
2. Z. Qin, T. Zhu, L. Chen, and X. Bao, "High sensitivity distributed vibration sensor based on polarization-maintaining configurations of phase-OTDR," IEEE Photonics Technol. Lett. **23**(15), 1091–1093 (2011).
3. A. H. Hartog and L. B. Liokumovich, "Phase sensitive coherent otdr with multi-frequency interrogation," U.S. patent WO2013066654 A1 (October 22, 2012).
4. Y. Dong, X. Chen, E. Liu, C. Fu, H. Zhang, and Z. Lu, "Quantitative measurement of dynamic nanostrain based on a phase-sensitive optical time domain reflectometer," Appl. Opt. **55**(28), 7810–7815 (2016).
5. R. Posey, G. A. Johnson, and S. T. Vohra, "Strain sensing based on coherent Rayleigh scattering in an optical fibre," Electron. Lett. **36**(20), 1688–1689 (2000).
6. A. Masoudi, M. Belal, and T. P. Newson, "A distributed optical fibre dynamic strain sensor based on phase-OTDR," Meas. Sci. Technol. **24**(8), 085204 (2013).
7. A. E. Alekseev, V. S. Vdovenko, B. G. Gorshkov, V. T. Potapov, and D. E. Simikin, "A phase-sensitive optical time-domain reflectometer with dual-pulse diverse frequency probe signal," Laser Phys. **25**(6), 065101 (2015).
8. Y. Shi, H. Feng, and Z. Zeng, "Phase-sensitive optical time domain reflectometer with dual-wavelength probe pulse," Int. J. Distrib. Sens. Netw. **11**(5), 624643 (2015).
9. J. P. Dakin and C. Lamb, "Distributed fibre optic sensor system," U.S. patent GB 2 222 247A (1990).
10. Z. Wang, Z. Pan, Z. Fang, Q. Ye, B. Lu, H. Cai, and R. Qu, "Ultra-broadband phase-sensitive optical time-domain reflectometry with a temporally sequenced multi-frequency source," Opt. Lett. **40**(22), 5192–5195 (2015).
11. D. Iida, K. Toge, and T. Manabe, "High-frequency distributed acoustic sensing faster than repetition limit with frequency-multiplexed phase-OTDR," in *Opt. Fiber Comm. Conf. and Exhibit. OFC* (2016), pp. 1–3.
12. Y. Koyamada, M. Imahama, K. Kubota, and K. Hogari, "Fiber-optic distributed strain and temperature sensing with very high measurand resolution over long range using coherent OTDR," J. Lightwave Technol. **27**(9), 1142–1146 (2009).
13. L. Zhou, F. Wang, X. Wang, Y. Pan, Z. Sun, J. Hua, and X. Zhang, "Distributed strain and vibration sensing system based on phase-sensitive OTDR," IEEE Photonics Technol. Lett. **27**(17), 1884–1887 (2015).
14. J. Pastor-Graells, H. F. Martins, A. Garcia-Ruiz, S. Martin-Lopez, and M. Gonzalez-Herraez, "Single-shot distributed temperature and strain tracking using direct detection phase-sensitive OTDR with chirped pulses," Opt. Express **24**(12), 13121–13133 (2016).

#280645 http://dx.doi.org/10.1364/OE.25.000720
Journal © 2017 Received 21 Nov 2016; revised 6 Jan 2017; accepted 9 Jan 2017; published 10 Jan 2017

Optics EXPRESS

## 1. Introduction

Conventional optical time domain reflectometry (OTDR) has long been a standard tool in the telecommunication industry for distributed fault detection and optical fiber loss characterization. Pulses of a rather incoherent optical source are used to avoid interference from the Rayleigh scattering along the fiber. However, probing the fiber with coherent pulses results in interference of the Rayleigh backscattered power from the distributed scattering centers (scatterers) along the fiber, resembling a distributed interferometer with a physical gauge length of half the pulse width in the fiber. The resulting jagged appearance of such a coherent OTDR (C-OTDR) trace is constant for static fiber condition but changes locally as the temporal relation between scatterers is changed as a function of applied temperature or strain changes. This technique is, depending on its implementation, also known as phase-OTDR /ϕ -OTDR or phase-sensitive OTDR and is used for distributed sensing over tens of kilometers. This so-called distributed vibration sensing (DVS), or distributed acoustic sensing (DAS), has found widespread application, among others, in the geophysical field, the oil and gas industry for borehole sensing or pipeline monitoring with high requirements on vibration sensitivity, frequency bandwidth or measurement distance. The remarkable performance of C-OTDR DVS has also attracted increasing interest from the structural health monitoring (SHM) sector. Our investigation targets this field, specifically the monitoring of transportation infrastructure such as bridges for distributed vibration mode analysis and the assessment of structural conditions. For distributed vibration mode shape analysis, it is essential not only to measure the correct amplitude of strain but also the algebraic sign of strain changes, which cannot be performed with most C-OTDR DVS approaches. The requirements on frequency bandwidth and strain resolution are lower for structural vibration analysis but the spatial resolution target of 1 m is more demanding than typically required for DVS applications.

Most of the proposed C-OTDR implementations for DVS can be allocated to one of three sub-groups: Direct-detection C-OTDR analyzes the directly detected Rayleigh backscatter interference along the fiber within the pulse duration [1]. The more complex coherent optical detection C-OTDR uses a high-coherence local oscillator and balanced detection to obtain phase information [2–4]. The third sub-group is based on the cross-multiply phase demodulation technique [5,6] which allows for the quantification of vibration amplitudes and frequencies. This technique has also been implemented in a direct-detection C-OTDR [7]. The coherent detection and cross-phase demodulation techniques require stabilization of additional interferometer(s) and balanced detection, increasing the overall complexity. Hence, it would be preferable to employ a measurement technique using a more simplified and robust direct-detection scheme.

Although various phase demodulation techniques have been implemented, determining the sign of strain or temperature signals is still an issue. In order to also measure the algebraic sign of changes in any interferometer, including C-OTDR, it is essential to analyze additional spectral information. We therefore propose to make full use of the information gained by sending pulses of different wavelengths into the fiber and analyzing relative Rayleigh backscatter power changes in a simple and robust direct-detection C-OTDR setup. The aim is to measure relative strain and temperature changes including the sign of the change.

Measuring with different pulse wavelengths in C-OTDR has been implemented in various ways. Most approaches, however, use the additional spectral information to improve the signal quality [8], increase the measurement repetition rate or conduct interferometric phase unwrapping. The first C-OTDR vibration measurement approach used a double pulse pair of slightly different wavelengths in direct detection [9]. Probing the fiber with multiple pulse frequencies in a heterodyne coherent-detection C-OTDR has also allowed to retrieve phase information and linearize the sensor strain response [3]. Furthermore, frequency-multiplexed pulses have been used in order to increase the maximum repetition rate limitation in C-OTDR sensing [10,11] but without using the extra spectral information. True relative strain or

Optics EXPRESS

temperature measurements including the correct algebraic sign have been demonstrated by Koyamada et al. [12] for precise but static strain and temperature measurements. This is achieved by correlating Rayleigh backscatter signatures in the backscatter-frequency plane with a previously recorded reference backscatter matrix. Similarly, Zhou et al [13] used multiple consecutive pulse frequencies and cross correlation in a direct-detection C-OTDR. Recently, the spectral information of frequency-chirped pulses in a direct-detection setup [14] have allowed for measuring temperature and strain changes including the sign using a high-bandwidth detection C-OTDR and correlating signal shifts along the fiber spatial domain.

Our approach is based on simple and robust direct-detection C-OTDR and requires little hardware configuration. Due to the measurement of relative backscatter changes with pulses of known wavelength (or frequency) difference, absolute changes as well as the sign of these changes can be determined. This is achieved by correlating the local backscattered power variations obtained at alternating pulse wavelengths along the signal axis (strain or temperature changes along the signal time axis) as opposed to correlating backscatter signal in the spatial domain [14] or in the frequency shift domain [12,13]. Compared to [12] and [13], the proposed dual-pulse wavelength evaluation allows for dynamic measurement and ensures a high vibration frequency detection bandwidth of half the Nyquist frequency (using classic single wavelength analysis) while maintaining minimal hardware requirements and using low-bandwidth photodiode and digitizers (as opposed to [14]) at the required high spatial resolution of 1 m.

This article is organized as follows: the proposed measurement method is theoretically described and visualized by means of a simulation in section 2. The proposed C-OTDR experimental setup is introduced in section 3. A temperature change measurement including sign change is demonstrated after a detailed description of the signal processing in section 4.

## 2. Theory and measurement method

Rayleigh scattering in silica optical fibers mainly originates from refractive index variations that became frozen in the fiber during the drawing process. Backscattering from a single mode fiber (SMF) can be described by a set of $N$ discrete scatterers with a uniform statistical distribution along the fiber axis $z$. The scatterers' specific reflectivities $r$ (with respect to optical power) can also be assumed to follow a uniform distribution. Both distributions are statistically independent. We assume that the fiber under test (FUT) is probed with a linearly polarized and fully monochromatic optical pulse of the duration $\tau_d$ and pulse peak power $I_0$ entering the fiber at the time $t = 0$. The total detected optical power $I(t)$ backscattered from the forward propagating pulse corresponds to the time-averaged and squared absolute value of the sum of the individual backscattered optical field components and is composed of an incoherent optical power component $I_{incoh}(t)$ and a coherent power component $I_{coh}(t)$:

$$\begin{aligned} I(t) &= \left| \sum_{i=1}^{N} \sqrt{r_i}\, \hat{E}_0 \mathrm{e}^{j2\pi\nu_0(t-\tau_i)} \mathrm{rect}\left( \frac{t-\tau_i}{\tau_d} \right) \right|^2 \\ &= I_{incoh}(t) + I_{coh}(t) = \sum_{i=1}^{N} r_i I_0 \mathrm{rect}\left( \frac{t-\tau_i}{\tau_d} \right) + I_{coh}(t) \end{aligned} \tag{1}$$

$\hat{E}_0$ and $\nu_0$ are the amplitude and frequency of the optical field, respectively, $\tau_i$ denotes the delay of the signal of the $i$th scatterer with $\tau_i = 2n_g z_i/c_0$, $c_0$ the speed of light, $n_g$ the fiber group refractive index and $z_i$ the position of the scatterer in the fiber. The propagating rectangular pulse is defined as $\mathrm{rect}([t-\tau_i]/\tau_d) = 1$ for $0 \le ([t-\tau_i]/\tau_d) \le 1$ and 0 otherwise. Scatterers within a fiber section corresponding to half the pulse width $w$ in the fiber with $w/2 = c_0\, \tau_d\, /(2n_g)$ contribute to the detected power. $w/2$ also defines the two-point spatial resolution of the sensor. The coherent power component $I_{coh}(t)$, as detected by a square-law polarization-

Optics EXPRESS

independent photodetector, can be described by a double summation of all scatterers' phase relations

$$I_{coh}(t)=\sum_{i=1}^{N-1}\sum_{e=i-1}^{N}2\sqrt{r_i r_e}I_0\cos\left[2\pi\nu_0\tau_{ie}\right]\mathrm{rect}\left(\frac{t-\tau_i}{\tau_d}\right)\mathrm{rect}\left(\frac{t-\tau_e}{\tau_d}\right) \tag{2}$$

with $\tau_{ie} = \tau_i - \tau_e = 2n_g z_{ie}/c_0$ being the scatterers' relative delay and $z_{ie} = z_i - z_e$ being the physical distance between the individual scatterers. Polarization preservation within $w/2$ is assumed and propagation loss is neglected. The phase term contains $\nu_0$ and $\tau_{ie}$ as factors. Changes of temperature $\Delta T$ and strain changes $\Delta\varepsilon = \Delta z_{ie} / z_{ie}$ along the fiber can be approximated to have a linear impact on the change $\Delta\tau_{ie}$ of the temporal delays $\tau_{ie}$ between the individual scatterers. This temporal change relation $\Delta\tau_{ie}/\tau_{ie}$ can be equivalently defined with respect to optical frequency difference relations $\Delta\nu/\nu_0$ or wavelength difference relation $\Delta\lambda/\lambda_0$ by means of the strain coefficient $K_\varepsilon \approx -0.78$ and the temperature coefficient $K_T \approx -6.92\cdot10^{-6}$ [12] for fiber Bragg gratings and standard SMF as

$$\begin{aligned}\frac{\Delta\nu}{\nu_0}&=-\frac{\Delta\lambda}{\lambda_0}=-\frac{\Delta\tau_{ie}}{\tau_{ie}}=-(1-p_e)\Delta\varepsilon=K_\varepsilon\Delta\varepsilon\approx-0.78\Delta\varepsilon\\ \frac{\Delta\nu}{\nu_0}&=-\frac{\Delta\lambda}{\lambda_0}=-\frac{\Delta\tau_{ie}}{\tau_{ie}}=-(\xi+\alpha)\Delta T=K_T\Delta T\approx-6.92\cdot10^{-6}\Delta T\end{aligned} \tag{3}$$

under the assumption that $|\Delta\tau_{ie}/\tau_{ie}| \ll 1$. $p_e \approx 0.22$ is the effective strain-optic constant of silica, $\xi$ is the thermo-optic coefficient of silica and $\alpha$ is the thermal expansion coefficient of the fiber. The impact that combined strain changes $\Delta\varepsilon$ and temperature changes $\Delta T$ have on the total delay changes $\Delta\tau_{ie}$ relative to the initial scatterer delays $\tau_{ie}$ can be substituted as

$$\tau_{ie}-\Delta\tau_{ie}=\tau_{ie}\left(1+K_\varepsilon\Delta\varepsilon+K_T\Delta T\right) \tag{4}$$

As indicated in Eq. (3), a relative frequency change $\Delta\nu$ has an equivalent impact on relative scatterers delay changes and can be inserted as the factor $(\nu_0 + \Delta\nu)$ in the phase term. Assuming that $\Delta T$ and $\Delta\varepsilon$ are uniform within $w/2$, their influences can be considered as additional factors in the phase term. The total optical power as a function of temperature changes $\Delta T(t_s)$ and strain changes $\Delta\varepsilon(t_s)$ over progressing time $t_s$ can then be described as

$$\begin{aligned}I\left(t,\Delta\varepsilon(t_s),\Delta T(t_s),\Delta\nu\right)=I_{incoh}(t)+\sum_{i=1}^{N-1}\sum_{e=i-1}^{N}2\sqrt{r_i r_e}I_0\\ \cdot\cos\left[2\pi(\nu_0+\Delta\nu)\tau_{ie}\left(1+K_\varepsilon\Delta\varepsilon(t_s)+K_T\Delta T(t_s)\right)\right]\\ \cdot\mathrm{rect}\left(\frac{t-\tau_i}{\tau_d}\right)\mathrm{rect}\left(\frac{t-\tau_e}{\tau_d}\right)\end{aligned} \tag{5}$$

Equation (5) shows that delay changes due to strain and temperature changes can be compensated by changes of the pulse optical frequency. The measurement approach is to use the linearity and interchangeability of the factors in the phase term to obtain temperature changes $\Delta T$ and strain changes $\Delta\varepsilon$ over time $t_s$ by alternatingly probing the FUT with pulses of a known frequency difference $\Delta\nu$ (or wavelength difference). In the experimental implementation, the power variations $I$ over $t_s$ as a function of $\Delta T(t_s)$ and $\Delta\varepsilon(t_s)$ are recorded with a pulse repetition frequency $f_p$ or pulse repetition period $\tau_p = 1/f_p$, respectively. The spatial sampling over $t$ (with $z = c_0 t/(2n_g)$) for each propagating pulse is performed at a sampling frequency $f_s$. The backscatter traces $I_{1,2}$ are sampled at alternating pulse optical frequencies $\nu_{1,2} = \nu_0 \pm \Delta\nu/2$ over the corresponding sampling time $t_{s1,2}$ (indexed due to alternating acquisition)

Optics EXPRESS

$$t_{s_{1,2}} = \frac{n_{1,2}}{f_p} \qquad \begin{matrix} \{n_1 \in \mathbb{N}_0 \mid n_1 \bmod 2 = 0\} \\ \{n_2 \in \mathbb{N}_+ \mid n_2 \bmod 2 = 1\} \end{matrix} \tag{6}$$

The indices $\{\cdot\}_{1,2}$ denote variables related to the pulse optical frequencies $\nu_1$ or $\nu_2$, with $\nu_1 > \nu_2$, or related parameters throughout this article. The total optical power $I_{1,2}(t,t_{s1,2})$ along the fiber axis (function of $t$) and along the signal axis (function of $t_{s1,2}$) is exemplarily simulated in Fig. 1 using Eq. (5) for a linearly increasing temperature $\Delta T(t_{s1,2}) = m_T\, t_{s1,2}$ with a temperature gradient $m_T$ = 20 mK/s and alternating pulse optical frequencies $\nu_{1,2}$. The simulation is conducted using parameters of the experimental C-OTDR implementation (section 3) with the following settings: $N$ = 10000 scatterers within $0 \le z_i \le 2c_0 \cdot 50\text{ns}/n_g$, $t = \tau_d + k/f_s$, $k \in \mathbb{N}_0$ and $k \le 45$, $f_s$ = 500 MHz, $\nu_0 = c_0$ /1.55 µm, $\tau_d$ = 10 ns, $\Delta\nu$ = 200 MHz, $m_T$ = 20 mK/s, $n_1 \le 5000$, $n_2 \le 4999$ and $f_p$ = 100 Hz.

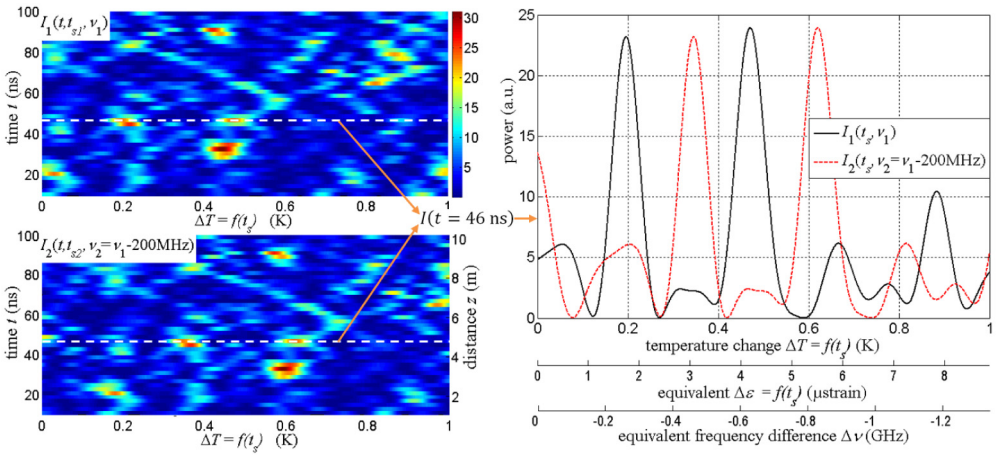


Fig. 1. Left: simulated power results $I_{1,2}(t,t_s,\nu_{1,2})$ as a function of temperature change $\Delta T(t_s)$ for two different pulse wavelengths ($N$ = 10000, $\nu_0 = c_0$/1.55 µm, $\tau_d$ = 10 ns, $\Delta\nu$ = 200 MHz) and right: power changes $I_{1,2}(t$ = 46 ns,$t_s)$ at $z \approx$4.7 m.

The simulation results show that $I_1$ is shifted relative to $I_2$ by a temperature change value $\Delta T(t_s)$ which is determined by $\Delta\nu$ according to Eq. (3). The similarity of $I_{1,2}$ may be degraded if significant polarization changes or strain/temperature change inhomogeneity occurs within the spatial resolution of $w$/2.

Our measurement approach is to use the similarity of measured backscatter traces $I_1$ and $I_2$ over progressing time $t_s$ to determine their temporal delay. From this temporal delay, unknown temperature variations $\Delta T(t_s)$ or strain changes $\Delta\varepsilon(t_s)$ can be determined. This is achieved by step-wise correlating overlapping sections of $I_1(t_s)$ and $I_2(t_s)$ to obtain signal shift over time $t_s$ and using the known relations from Eq. (3) to determine relative strain or temperature change values. The correlation algorithms and signal processing applied to C-OTDR measurement results are presented in detail in section 4 before a temperature change measurement of a FUT section is demonstrated in section 5. But first, the implementation of the experimental setup is introduced in detail.

## 3. Experimental setup

The experimental setup, as shown in Fig. 2, is based on the direct-detection C-OTDR architecture to avoid polarization issues and additional interferometers in the optical path. It is designed to generate short pulses of $\tau_d$ = 10 ns with a corresponding spatial resolution of 1m. A low-cost DFB laser diode with a linewidth of 1.1 MHz and center wavelength of $\lambda_0$ =

Optics EXPRESS

1550.116 nm ($\nu_0$ = 193.405 THz) was used for the experiments. With a coherence length of 59 m in the fiber, sufficient degree of coherence within the pulse width is maintained.

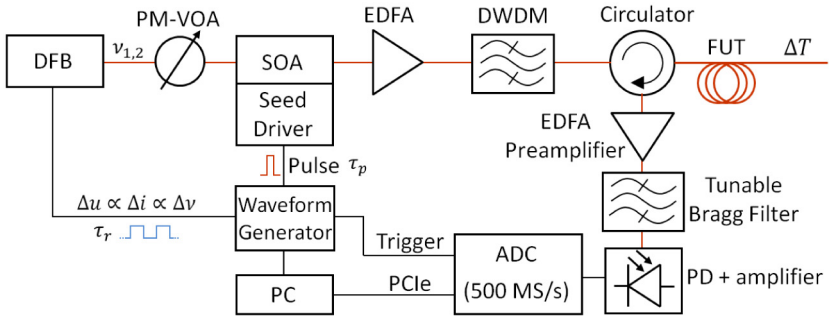


Fig. 2. Schematic of the dual-wavelength direct-detection C-OTDR setup.

A semiconductor optical amplifier (SOA) is used as a fast optical switch to generate short pulses with a high extinction ratio (nominally 70 dB). The input power into the SOA is adjusted by a polarization-maintaining variable optical attenuator (PM-VOA). A 120 MHz waveform generator supplies the pulse signal via a seed driver. The generated pulses are amplified to several hundred mW peak power using an erbium-doped fiber amplifier (EDFA). After filtering the amplified spontaneous emission (ASE) noise with a 0.2 nm bandwidth dense wavelength-division multiplexing (DWDM) filter, the pulses are coupled into a standard single mode FUT via a polarization-insensitive optical circulator. The backscattered power is amplified by an EDFA preamplifier and is filtered with a narrow linewidth (3 GHz) Bragg filter (similar results can be obtained with a 0.2 nm DWDM filter) before being detected by a 125 MHz bandwidth PIN photodetector with an integrated transimpedance amplifier. The backscatter signal is sampled by a 500 MS/s analog-to-digital converter (ADC). The acquisition with 14 bit resolution is triggered by the waveform generator. This sampling rate translates to a spatial sampling every 20 cm along the fiber, smaller than the 1 m spatial resolution (overlapping sensor sections). The measurement repetition rate is only limited by the fiber length $z_{max}$ with $f_p = c_0/(2n_g z_{max})$. A pulse repetition rate of $f_p$ = 2 MHz can for example be recorded at the full 500 MS/s up to $z_{max}$ ≈51 m. The generation of frequency-shifted pulses is implemented with minimal hardware expenses: the laser current-wavelength dependency of the DFB laser is used to shift the emission wavelength of the pulses to $\nu_{1,2} = \nu_0 \pm \Delta\nu/2$ by superimposing a synchronized rectangular voltage modulation of $\mp \Delta u/2$ and a period of $\tau_r = 2\tau_p$ onto the constant-current laser controller, as depicted in Fig. 3 (left). Figure 3 (right) shows two backscatter traces $I_{1,2}(z)$ of a 1012 m long FUT with deviating power values due to the measurement at different pulse wavelengths.

Optics EXPRESS

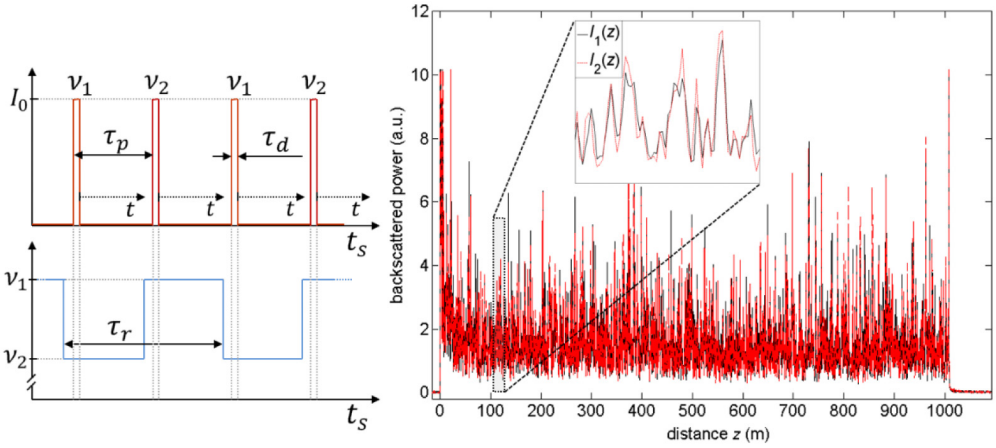


Fig. 3. Sketch of the dual-wavelength scheme (left) and measured C-OTDR traces $I_{1,2}(z)$ at different pulse optical frequencies with $\Delta\nu \approx 34$ MHz (right)

The laser frequency shift has been measured using the delayed self-heterodyne technique. It exhibits a linear dependence on the modulation voltage $\Delta u$ with a slope of $\Delta\nu/\Delta u \approx$- 17 MHz/mV. The current dependency of about $\Delta i/\Delta u \approx$20 µA/mV translates to $\Delta\nu/\Delta i \approx$- 0.75 MHz/µA and a negligible optical power change of $\log_{10}[(I_0 + \Delta I_0)/I_0]/\Delta\nu \approx$0.006 dB/100 MHz. The emission frequency stability of the source may be an accuracy limiting factor for long-term change measurement. The calculated frequency stability of the DFB laser in combination with the temperature controller over 24 hours is in the order of 18 MHz (equivalent to strain/temperature changes of ± 120 nε and ± 13.4 mK, respectively).

## 4. Signal processing

Assuming uniform temperature and strain changes within $w/2$, the detected power variations $I_{1,2}(t_s)$ during strain change $\Delta\varepsilon(t_s)$ or temperature change $\Delta T(t_s)$ exhibit a similar variation but are delayed in time $t_s$ (compare to Fig. 1). This delay corresponds to the $\Delta\nu$-dependent factors $\Delta p_T$ for temperature and $\Delta p_\varepsilon$ for strain, respectively:

$$\Delta p_T = \frac{\Delta\nu}{\nu_0}\frac{1}{K_T} \qquad \Delta p_\varepsilon = \frac{\Delta\nu}{\nu_0}\frac{1}{K_\varepsilon} \tag{7}$$

By calculating this time delay (or shift) $\Delta t(t_s)$ for the progressing time $t_s$, temperature and strain gradients $m_T(t_s)$ and $m_\varepsilon(t_s)$ can be obtained as

$$m_T(t_s) = \frac{\Delta p_T}{\Delta t(t_s)} \qquad m_\varepsilon(t_s) = \frac{\Delta p_\varepsilon}{\Delta t(t_s)} \tag{8}$$

This is achieved by applying a cross-covariance algorithm to overlapping sections of measured power results $I_{1,2}(t_s)$ with a 'correlation window length' corresponding to the correlation period $\tau_c$ ($\tau_c$ being an integer multiple of $\tau_r$). The correlation results can be improved by averaging the measured $I_{1,2}(t_{s1,2})$ results over $a$ results as

$$\bar{I}_{1,2}\left(t_{s_{1,2}}\right) = \frac{1}{a}\sum_{i=-\frac{a-1}{2}}^{\frac{a-1}{2}} I_{1,2}\left(t_{s_{1,2}} + i\tau_r\right) \tag{9}$$

$$\text{with } a \text{ odd}, a \geq 3 \text{ and } t_{s_{1,2}} \geq \frac{a-1}{2}\tau_r$$

Optics EXPRESS

The 'correlation window' is shifted in time steps of $\tau_{shift} < \tau_c$ so that averaged delay results are calculated for overlapping correlation windows ($\tau_{shift}$ being an integer multiple of $\tau_r$). A temporal shift vector $\Delta t(t_s')$ at the time $t_s' = a\tau_r + \tau_c/2 + k\tau_{shift}$ with $k \in \square_0$, $k < [\max(t_s) - a\tau_r - \tau_c]/\tau_{shift}$ is derived directly from the position of the maximum of the cross-covariance function of the correlated sections with $\bar{I}_1(t_{s1})$ and $\bar{I}_2(t_{s2})$ as input. The calculated temporal shift result $\Delta t(t_s')$ represents an averaged shift value within the sliding 'correlation window':

$$\Delta t\left(t_s'\right) = \left[\underset{t_s'}{\operatorname{argmax}}\left(\operatorname{cov}\left\{\bar{I}_1\left(t_{s_1}\right), \bar{I}_2\left(t_{s_2}\right)\right\}\right) - 1\right]\tau_r - \tau_c - \tau_p$$
$$\text{with } t_s' - \frac{\tau_c}{2} \le t_{s_{1,2}} < t_s' + \frac{\tau_c}{2} \tag{10}$$

where $\operatorname{cov}\{\bar{I}_1(t_{s1}), \bar{I}_2(t_{s2})\}$ denotes the cross-covariance function of the input vectors $\bar{I}_1(t_{s1})$ and $\bar{I}_2(t_{s2})$, and is the argument of the maximum position. The temporal shift $\Delta t(t_s')$ can then be used to calculate the temperature or strain gradients $m_{T,\varepsilon}(t_s')$ using Eq. (8). The resulting temperature change $\Delta T(t_s')$ or strain change $\Delta\varepsilon(t_s')$ corresponds to the cumulative sum of gradients and is calculated by inserting Eq. (8) as

$$\Delta T\left(t_{s_i}'\right) = \sum_{j=0}^{i} \tau_{shift} \frac{\Delta p_T}{\Delta t\left(t_{s_j}'\right)} \qquad \Delta\varepsilon\left(t_{s_i}'\right) = \sum_{j=0}^{i} \tau_{shift} \frac{\Delta p_\varepsilon}{\Delta t\left(t_{s_j}'\right)} \tag{11}$$

with $t_{s_j}'$ and $t_{s_i}'$ being elements of $t_s'$. For simplicity reasons, $t_{s_i}'$ is from here on simply denoted as $t_s$. The $\Delta T(t_s)$ and $\Delta\varepsilon(t_s)$ results comprise relative change values including the algebraic sign of change. The cumulative sum result from Eq. (11) comprises an accumulated error of the change values from Eq. (8). However, it can be assumed that the deviation of the gradient in Eq. (8) approximately exhibits a symmetric distribution (error) around the actual gradient. In analogy to the expected value in any symmetric probability distribution around zero, the cumulative sum results from Eq. (11) converge to the correct change result. Any physical effect or signal processing effect distorting the gradient error symmetry will cause an accumulated deviation from the correct change result.

## 5. Experimental results

To demonstrate the proposed technique, C-ODTR measurements during a temperature change at the end of a 1012 m long standard single mode FUT (Fig. 3, right) have been recorded: A 20 m long fiber section was placed in a water basin which was heated and subsequently cooled down while measuring $I(t,t_s)$. By applying Eq. (7)–11) to the measured C-OTDR data, the fiber's relative temperature change results are retrieved. Figure 4 shows $\bar{I}_{1,2}(t_s,z = 1001.1$ m) during monotonous temperature increase (left) and the resulting temperature change (right) of three adjacent sampling points $\Delta T(t_s,z)$ at $z = 1000.7$ m, $z = 1000.9$ m and $z = 1001.1$ m (partially overlapping 1 m sensor sections). For comparison, a temperature measurement trace recorded by a thermistor is added to the plot. The measured temperature changes $\Delta T(t_s,z)$ are adjusted to the initial thermistor temperature value.

Optics EXPRESS

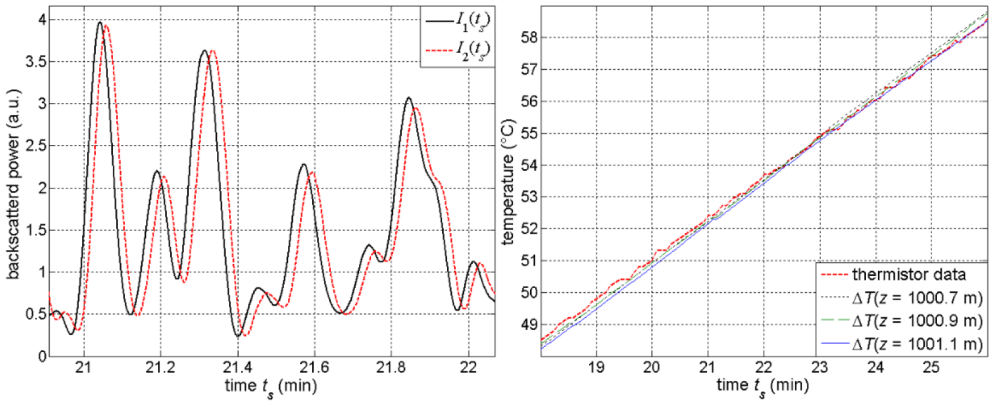


Fig. 4. Measurements: increasing temperature $\bar{I}_{1,2}(t_s,z$ = 1001.1 m) (left) and $\Delta T(t_s,z)$ at $z$ = 1000.7 m, $z$ = 1000.9 m and $z$ = 1001.1 m during increasing temperature (right), ($\tau_d$ = 10 ns, $\Delta\nu$ ≈ 34 MHz, $a$ = 19, $f_p$ = 5 kHz, $\tau_c$ = 150 s, $\tau_{shift}$ = 5 s).

The similarity of $\bar{I}_{1,2}$ is clearly visible with $\bar{I}_1$ being delayed by $\Delta t(t_s)$ relative to $\bar{I}_2$ during temperature increase. The lag or delay equivalent to the frequency difference of $\Delta\nu \approx 34$ MHz corresponds to a temperature difference of 25.4 mK and a strain change of 0.228 με, respectively. The similarity of $\bar{I}_{1,2}$ may be degraded if significant polarization changes or strain/temperature change inhomogeneities occur within $w/2$. Figure 5 (left) shows the detected backscatter changes $\bar{I}_1(t_s)$ during heating and subsequent cooling of the fiber for $t_s >$ 46 min. The lag of $\bar{I}_2$ relative to $\bar{I}_1$ implies a negative temperature gradient. The temperature change evaluation in Fig. 5 (right) is consistent with the thermistor results and clearly demonstrates that also the sign change can be correctly measured after the heating stopped and the temperature decays.

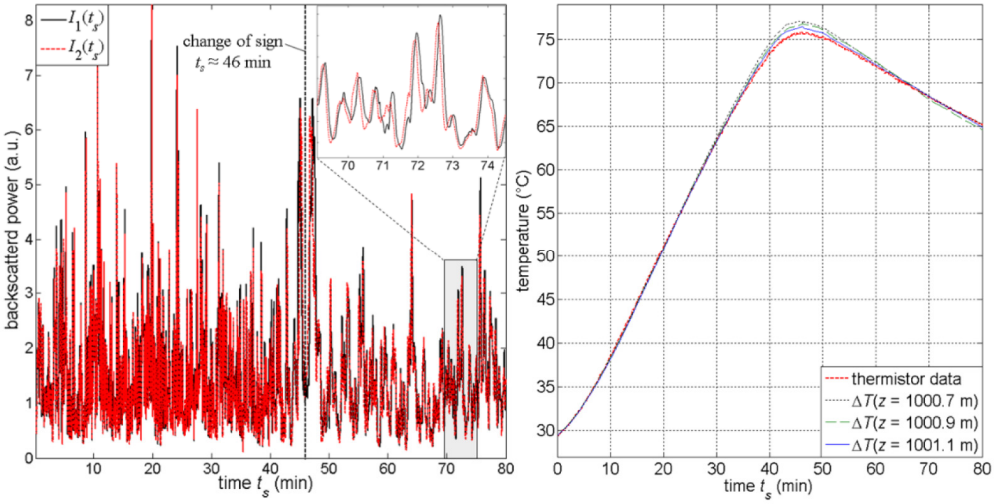


Fig. 5. Measurement results, left: $\bar{I}_{1,2}(t_s,z$ = 1001.1 m) and right: $\Delta T(t_s)$ at $z$ = 1000.7 m, $z$ = 1000.9 m and $z$ = 1001.1 m during heating and cooling of the fiber ($\tau_d$ = 10 ns, $\Delta\nu \approx$ 34 MHz, $a$ = 19, $f_p$ = 5 kHz, $\tau_c$ = 150 s, $\tau_{shift}$ = 5 s).

The small deviations of the thermistor point sensor results are mainly due to inhomogeneities of the temperature distribution in the water during the temperature change. The measurement proves that the proposed technique is suitable for accurately tracking changes of temperature and can also be applied for strain change measurement. It also demonstrates that the sign of the change can be correctly determined.

Optics EXPRESS

## 6. Conclusion

We have proposed, to our knowledge for the first time, a distributed temperature and strain change measurement technique by using the spectral information of a dual-wavelength direct-detection C-OTDR and correlating the delay of pulse wavelength-dependent power variations along the signal (temperature/strain) axis. A stable pulse wavelength shift has been implemented by simple laser current modulation of a standard telecom DFB laser in a cost-effective direct-detection C-OTDR architecture. The demonstrated 1 m spatial resolution is sufficient for many SHM applications and the intended distributed vibration mode analysis. Absolute temperature change measurement including the correct algebraic sign has been experimentally demonstrated. This approach can be analogously used for strain change and vibration measurement while maintaining the high frequency detection bandwidth capabilities of conventional C-OTDR at half the Nyquist frequency. The sensing scheme can be easily extended to measure with more than two wavelengths to improve the correlation results at reduced vibration detection bandwidth. Our implementation is capable of measuring at a fiber length-limited pulse repetition rate exceeding 2 MHz. A practical vibration measurement using the proposed dual pulse wavelength technique is expected to reach hundreds of Hz. The next step is to use this technique for distributed vibration measurement and develop efficient adaptive correlation algorithms.

## Funding

BAM Themenfeld project “Bewertung, Lebensdauerprognose und Instandsetzung von Brückenbauwerken” (BLEIB).

## Acknowledgments

We are thankful for the financial support and the fruitful cooperation with all partners.